Available online at www.sciencedirect.com
ScienceDirect
International Journal of Heat and Mass Transfer 50 (2007) 5260–5268
International Journal of HEAT and MASS TRANSFER
www.elsevier.com/locate/ijhmt

Assessment of simplified thermal radiation models for engineering calculations in natural gas-fired furnace

D.A. Kontogeorgos, E.P. Keramida, M.A. Founti *

Department of Mechanical Engineering, National Technical University of Athens, Zografou Campus, Athens 157 80, Greece

Received 25 January 2007
Available online 13 August 2007

Abstract

The paper assesses the significance of thermal radiation in turbulent non-premixed natural gas flames confined in axisymmetric furnaces. The in–house developed computational model includes simulation of the turbulent flow characteristics, the controlling mixing and chemical mechanisms as well as radiation modeled via the six-flux and of the P-1 models. A variable absorption coefficient is taken into account for the gaseous combustion mixture based on temperature and composition of the mixture. The results with and without radiation are evaluated as part of the complete prediction procedure involving flow, combustion, convection, and radiation phenomena. The comparative assessment of the two radiation models against experimental data indicates that they can be easily applied in engineering cases, with the P-1 model yielding more accurate results in the case considered.

Keywords: Radiation; Natural gas furnaces; Six-flux model; P-1 model

1. Introduction

Thermal radiation in gaseous media can be an important mode of heat transfer in high temperature combustion systems, such as combustors, furnaces and fires. Radiation exchange plays a very important role even under non-soot conditions. In hydrocarbon fuel combustion, products like H_2O, CO_2, CO are especially significant due to their high absorptivities and emissivities that drastically affect heat transfer characteristics and emphasize the need for evaluation of their effects on radiative heat transfer.

Although computational fluid dynamics (CFD) has become a widely used and reliable tool to support researchers and designers in the characterization, understanding and optimization of energy devices, radiation is often neglected among the complex flow, thermo-kinetic and convection phenomena. This is primarily associated with the high computational cost linked with the solution of the radiation equations, the significant uncertainty in relation to the properties of the participating media and the optical properties of involved surfaces. However, ignoring radiation may introduce considerable inaccuracies in the overall predictions. For example, thermal radiation affects the structure and extinction characteristics of hydrocarbon fuels [1,2], as well as the NO formation due to the sensitivity of thermal NO kinetics to temperature (which is very important to air pollution) [3–5].

Several analytical methods have been developed to support the engineering treatment of radiative heat transfer. Radiation models are mostly tested separately, in isolation of other physical processes [6–9]. Nevertheless, in real combustion systems where non-uniform velocity and temperature distributions occur, the predictive behavior of any radiation model is expected to differ from the simplified case [6,10]. The most precise model categories are

* Corresponding author. Address: Laboratory of Heterogeneous Mixtures and Combustion Systems, Thermal Engineering Section, School of Mechanical Engineering, National Technical University of Athens, Heroon Polytechniou 9, Polytechnioupoli-Zografou, Athens 157 80, Greece. Tel.: +30 210 772 3605; fax: +30 210 772 3663.
E-mail address: mfou@central.ntua.gr (M.A. Founti).

0017-9310/$ - see front matter © 2007 Elsevier Ltd. All rights reserved.
doi:10.1016/j.ijheatmasstransfer.2007.06.011

Nomenclature

A	reaction rate constant
A_j	pre-exponential factor
B	reaction rate parameter
B_j	backward rate constant of reaction j
C	linear-anisotropic phase function coefficient
E	emissive power (W m^{-2})
E_j	activation energy (J kmol^{-1})
e_w	surface emissivity
F_j	forward rate constant of reaction j
G	incident radiation (W m^{-2})
$[I]$	molar concentration of component I (kmol)
k	turbulence kinetic energy (m^2 s^{-2})
N_C	number of components
N_R	number of reactions
q_r	radiation flux (W m^{-2})
R	universal gas constant, 8314 (J kmol^{-1} K^{-1})
R_j	elementary reaction rate of progress for reaction j (kmol s^{-1})
S_I	rate of production/consumption for the component I (kg s^{-1})
S_Φ	source term
S_{rad}	radiative energy boundary source term (W m^{-2})
T	temperature (K)
t	time (s)
x, r	co-ordinate axes in cylindrical geometry
$\vec{U}$	velocity (m s^{-1})
W_I	molecular weight of component I (kg kmol^{-1})
Y_I	mass fraction of component I (kg kg^{-1})

Greek symbols

α	gas absorption coefficient (m^{-1})
β_j	temperature exponent
Γ_Φ	diffusion coefficient
ε	dissipation of turbulence energy (m^2 s^{-3})
v_{jI}	stoichiometric coefficient for component I in the elementary reaction j
ρ	density (kg m^{-3})
σ	Stefan–Boltzmann constant, 5.67×10^{-8} (W m^{-2} K^{-4})
σ_s	gas scattering coefficient (m^{-1})
Φ	transport variable

Subscripts

I	component
j	reaction
kin	kinetically controlled
mix	mixing controlled
r	radial direction
w	wall
x	axial direction

Superscripts

$\sim$	favre averaging
P	products
R	reactants

considered to be the zone [11], the Monte Carlo [12] and the flux [13] models. The first two require significant computational time and storage and they are not used very often for engineering calculations. Flux methods are easy to understand, readily applicable, fast and have successfully been applied to a number of confined cases, e.g. [14–16].

The present study intents to complement the previous work of Keramida et al. [14] that examined numerically a turbulent, non-premixed, natural gas flame with and without consideration of the radiation effects by using the six-flux and the discrete transfer model. The results demonstrated the importance of thermal radiation on flame temperature predictions. Both examined radiation models, performed similarly showing good agreement with the experimental data. The results indicated that the modeler could take advantage of the simplicity and low computational requirement of the six-flux model and use it with confidence for describing the radiative heat transfer in natural gas-fired furnaces.

The six-flux is a differential model providing convenience in the discretization of the transport equations but accounts for contributions to the radiative flux coming from only six directions; parallel and anti-parallel to the three main coordinate directions [17,18]. It retains the important parameters relevant to the case scenarios, although it assumes that radiation is transmitted only in the coordinate directions. It also offers computational economy and solves directly on the flow spatial grid, which means that there is no need for special description of the geometry. On the other hand, it has no inter-linkages, apart from scattering, between the radiation fluxes in the respective coordinate directions. It is quite accurate for optical thick media, but it will yield inaccurate results for thinner (transparent) media, especially near boundaries, and also if the radiation field is anisotropic. Finally, it fails in cases of complex geometry, such as congested spaces, or many and large openings.

In this study another radiation model is tested versus the six-flux model, namely the P-l model [19,20]. The P-1 is a simplification of the spherical harmonics method, and has recently gained acceptance as it can deliver good accuracy in optical thick media, such as combustion applications. This approximation is considered a popular method since it reduces the equation of radiative transfer from a very complicated integral equation to a relatively simple partial differential equation. The P-1 approximation is powerful and the average heat transfer engineer is much better trained in solving differential equations than integral equations. Furthermore, if overall energy conservation is com-

puted, compatibility of the solution methods is virtually assured. However it is important to remember that the model may produce substantial error in optically thin situations, in particular in multi-dimensional geometries with large aspect ratios (i.e. long and narrow configurations) and/or when surface emission dominates over medium emission [19,20]. The P-1 model requires limited CPU demand [4] and, as a result, can be easily applied.

The present study compares the performance of the P-1 and 6-flux radiation models. Numerical experiments are carried out in a natural gas fired furnace using the above two radiation models and the results are compared to the non-radiation model case. The computed temperature fields are compared to experimental data provided by the 'Delft experiment' [21], which is a flow characterized by steep temperature gradients. The flame is stabilized with the aid of pilot flames. The complexity of the flow and the availability of detailed experimental data make the case appropriate for the assessment of the above radiation models.

2. The physical and mathematical model

2.1. Furnace configuration

The case studied is a typical chamber of gaseous combustion, namely a cylindrical enclosure of 293 mm radius and 990 mm length [21]. The fuel is injected from a central jet, whereas the primary air supply enters from an annulus. The secondary airflow is inserted axially in the direction of the primary air-supply from a second annulus. The pilot flames are created via 12 holes (0.5 mm in diameter) circumferentially located on an imaginary ring at 3.5 mm from the centre of the burner. They are used to stabilize the natural gas flame and are fuelled by a mixture of acetylene, hydrogen and air, where the ratio of the flow rates of acetylene and hydrogen was chosen to give the same C–H ratio as in the natural gas and not affecting the chemistry of the turbulent flame. The overall geometry of the burner is illustrated in Fig. 1. The inlet conditions for the fuel and air (primary and secondary) are shown in Table 1. The presence of the pilot flames introduces an additional complexity in the computational procedure. They are simulated in such a way as to guarantee ignition, but minimizing their effect on the general flow pattern. The 12 holes are replaced by a concentric slit burner fed by burnt gases, giving a mass flow rate equal to that one achieved in the experiment according to the specification of Table 2 (see Fig. 2).

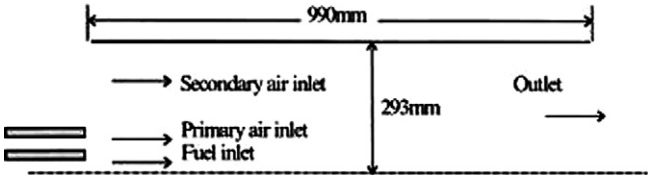

Fig. 1. Geometry of the chamber.

Table 1
Input conditions and fluid properties

Geometry			
Fuel inlet zone (mm)	From $r = 0.0$ to $r = 3.0$		
Primary air inlet zone (mm)	From $r = 7.5$ to $r = 22.5$		
Secondary air inlet zone (mm)	From $r = 22.5$ to $r = 293.0$		
Burner radial (mm)	293.0		
Burner length (mm)	990.0		
	Fuel inlet	Primary air	Secondary air
Inlet boundary conditions			
Axial velocity (m/s)	21.9	Fig. 2	0.3
Radial velocity (m/s)	0.0	0.0	0.0
Turbulent kinetic energy (m^2/s^2)	2.2	Fig. 2	0.0004
Dissipation of turbulence (m^2/s^3)	500	Fig. 2	0.0002
Temperature (K)	295	295	295
	Air	Fuel (Groningen natural gas)	
Composition (mass fraction)			
O_2	0.2315	0.0	
N_2	0.7685	0.2152	
CH_4	0.0	0.7638	
CO_2	0.0	0.0210	

Table 2
Conditions for pilot flames simulation

Inner radius (mm)	3.5		
Outer radius (mm)	4.0		
Inlet velocity (m/s)	17.9		
Temperature (K)	2220		
Composition (mass fraction)	CO_2	H_2O	N_2
	0.15	0.12	0.73

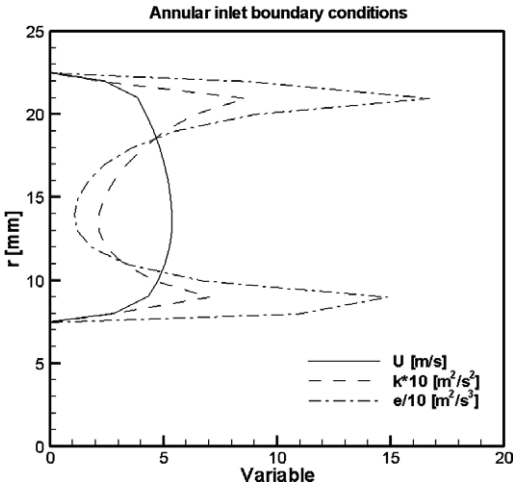

Fig. 2. Annular inlet boundary conditions.

2.2. Mathematical model

A two dimensional CFD code developed in the Laboratory of Heterogeneous Mixtures and Combustion Systems [22] is used in order to simulate the flow and chemical reactions in the combustor chamber. The in-house *2PHASE*

code is conceptually developed for the modelling of multi-phase, multi-component, reacting flows (using both Euler–Lagrange and Euler–Euler formulations). The code is purposely kept as simple as possible – maintaining a good physical representation of the main phenomena – in order to be used for assessment of detailed models pertaining to complex flows and not to "mask" the impact of each individual model. It has been previously validated in a number of gas–particle, liquid–particle, gas–liquid flows with and without chemical reaction [23,24,28,29].

The gaseous phase is treated via partial differential equations describing the conservation of momentum, heat and mass, in conjunction with a two-equation turbulence model. The ensuing system of mass, momentum, species and energy conservation equations is expressed in the general form of Eq. (1). Φ stands for the dependent variables, Γ_Φ is the transport coefficient of variable Φ and S_Φ is the source term of the transport equation for Φ including the rate of generation of the chemical species, the rate of heat generation and the rate of heat transfer with radiation. The above system is solved via a finite volume method based on a staggered grid arrangement, using the SIMPLE algorithm [25]. The turbulence kin etic energy and the dissipation of turbulence are calculated with the standard k–ε model [26]. Standard wall functions are used for the near-wall boundary conditions; convective heat transfer phenomena are also taken into account [27].

$$\frac{\partial}{\partial t}(\rho\Phi) + \nabla\cdot(\rho\vec{U}\Phi - \Gamma_\Phi\nabla\Phi) = S_\Phi \tag{1}$$

2.3. The combustion model

In general, chemical reactions can be described in terms of N_R elementary reactions involving N_C components that can be written as shown in Eq. (2).

$$\sum_{I=A,B,C}^{N_C} V'_{jI} I \Longleftrightarrow \sum_{I=A,B,C}^{N_C} V''_{jI} I \tag{2}$$

where v_{jI} is the stoichiometric coefficient for component I in the elementary reaction j.

The rate of production/consumption, S_I, for the component I can be computed as the sum of the rate of progress for all the elementary reactions that component I participate in Eq. (3).

$$S_I = W_I \sum_{j=1}^{N_R} (V''_{jI} - V'_{jI}) R_j \tag{3}$$

where R_j is the elementary reaction rate of progress for reaction j and W_I the molecular weight of component I.

A suitable turbulent combustion model is required in order to determine this reaction rate, which allows the calculations of the source terms in the species and enthalpy transport equations. The combustion process is here simulated using the combined eddy-dissipation/finite rate combustion model. According to the model, in the mixing-controlled regime, the reaction rate R_{mix} is calculated using the eddy-dissipation model [30], while in the kinetically controlled regime the reaction rate R_{kin} is calculated according to an Arrhenius formula [31,32]. For each computational cell the reaction rate is set as the minimum of R_{mix} and R_{kin}.

The eddy-dissipation model is based on the concept that chemical reaction is fast relative to the transport processes in the flow. When reactants mix at the molecular level, they instantaneously form products. The reaction rate is proportional to the inverse of the time-scale of the large-scale eddies characterized by the ration k/ε and to the smallest of the fuel, oxygen or products concentration. The rate of progress of the elementary reaction j is determined by the minimum of a reactants and products limiter (Eq. (4)).

$$R_j = \min(R_j^R, R_j^P) \tag{4}$$

The reactants limiter is defined from Eq. (5).

$$R_j^R = A\frac{\tilde{\varepsilon}}{\tilde{k}}\min\left(\frac{[I]}{V'_{jI}}\right) \tag{5}$$

where $[I]$ is the molar concentration of component I, which only includes the reactants, while the products limiter is determined from Eq. (6).

$$R_j^P = AB\frac{\tilde{\varepsilon}}{\tilde{k}}\min\left(\frac{\sum_P [I]W_I}{\sum_P V''_{jI} W_I}\right) \tag{6}$$

where P loops over all product components in the elementary reaction j. A, B are constants which take the values of 4 and 0.5, respectively.

The finite rate chemistry model assumes that the rate of progress of the elementary reaction j can be reversible only if a backward reaction is defined. Therefore, the rate of progress is determined by Eq. (7).

$$R_j = \left(F_j \prod_{I=A,B,C}^{N_C} [I]^{r'_{jI}} - B_j \prod_{I=A,B,C}^{N_C} [I]^{r''_{jI}}\right) \tag{7}$$

F_j and B_j are the forward and backward rate constants defined by Eqs. (8) and (9) and r represents the reaction order of the component I in the elementary reaction j.

$$F_j = A_j T^{\beta_j} \exp\left(-\frac{E_j}{RT}\right) \tag{8}$$

$$B_j = A_j T^{\beta_j} \exp\left(-\frac{E_j}{RT}\right) \tag{9}$$

A_j is the pre-exponential factor, β_j is the temperature exponent (dimensionless), E_j is the activation energy and T is the absolute temperature.

In the present study, combustion is modelled as a two-step mechanism, where production and combustion of carbon monoxide is taken into account. In the first stage, fuel is oxidized into carbon monoxide and water vapour, while in the second stage carbon monoxide oxidizes into carbon dioxide (Eqs. (10) and (11)).

$$CH_4 + \frac{3}{2}O_2 \rightarrow CO + 2H_2O \quad (10)$$

$$CO + \frac{1}{2}O_2 \rightarrow CO_2 \quad (11)$$

2.4. Radiation models

2.4.1. The P-1 model

In the present formulation of the P-1 model, four terms in the series expansion are used and Eq. (12) is obtained for the radiation flux q_r.

$$q_r = -\frac{1}{3(\alpha+\sigma_s) - C\sigma_s}\nabla G \quad (12)$$

where α is the absorption coefficient, σ_s is the scattering coefficient, G is the incident radiation and C is the linear-anisotropic phase function coefficient. It ranges from -1 to $+1$ and represents the amount of radiation scattered in forward direction. A positive value indicates that more radiant energy is scattered forward than backward with $C = 1$ corresponding to complete forward direction. A negative value means that more radiant energy is scattered backward than forward with $C = -1$ standing for complete backward scattering. A zero value of C defines isotropic scattering. This approximation is implemented in the present study.

The transport equation for G is show in Eq. (13).

$$\nabla\left(\frac{1}{3(\alpha+\sigma_s) - C\sigma_s}\nabla G\right) - \alpha G + 4\alpha\sigma T^4 = 0 \quad (13)$$

where σ is the Stefan–Boltzmann constant. Combining Eq. (12) and (13), Eq. (14) is obtained where the expression for radiation's flux gradient can be directly substituted into the energy equation to account for heat sources or sinks due to radiation.

$$-\nabla q_r = \alpha G - 4\alpha\sigma T^4 \quad (14)$$

The flux of the radiation at walls, $q_{r,w}$, caused by incident radiation G_w is given from Eq. (15) and e_w is wall emissivity.

$$q_{r,w} = -\frac{e_w}{2(2-e_w)}(4\sigma T_w^4 - G_w) \quad (15)$$

2.4.2. The six-flux model

The model employs diffusion-type differential equations for calculating radiative heat transfer. The solid angle surrounding a point is divides into six solid angles. The following second-order ordinary differential equations describe in polar coordinates the six-flux model, for a two-dimensional case (actually a four-flux):

$$\frac{1}{r}\frac{d}{dr}\left[\frac{1}{\alpha+\sigma_s+\frac{1}{r}}\frac{d(R_r)}{dr}\right] = R_r(\alpha+\sigma_s) - \alpha E - \frac{\sigma_s}{2}(R_r + R_x) \quad (16)$$

$$\frac{d}{dx}\left[\frac{1}{\alpha+\sigma_s}\frac{d(R_x)}{dx}\right] = R_x(\alpha+\sigma_s) - \alpha E - \frac{\sigma_s}{2}(R_r + R_x) \quad (17)$$

R_r, R_x are the composite radiative fluxes in radial and axial directions respectively. Each of the differential flux equations expresses the attenuation of a flux with distance as a result of absorption and scattering and its augmentation by emission and scattering from other directions.

The required boundary source term, S_{rad}, for a wall is:

$$S_{rad} = \frac{e_w}{2-e_w}(E_w - R_w) \quad (18)$$

where $E_w = \sigma T_w^4$, is the emissive power on the wall, e_w is the emissivity constant on the wall and R_w is the radiation flux near the wall.

At symmetry planes and perfectly reflecting boundaries, the radiative heat flux is zero. At non-reflecting boundaries, such as openings or free boundaries, the outgoing radiation leaved the computational domain without reflection.

3. Computational details

The computations were performed both on a 194 (axial) × 86 (radial) and a 288 × 172 mesh in order to secure grid independence. The results were virtually identical. The grid lines were non-uniformly spaced on both radial and axial direction as shown in Fig. 3.

The walls were treated as a grey heat sink of emissivity 0.8 and assumed to be completely water-cooled at a temperature of 295 K [21]. Wall scattering coefficient is taken 0.01 m^{-1}. Curve fits for the Planck mean absorption coefficients for H_2O, CO_2, CH_4 and CO were used as functions of temperature produced from the RADCAL program as shown in Fig. 4 [33]. The RADCAL program predicts the

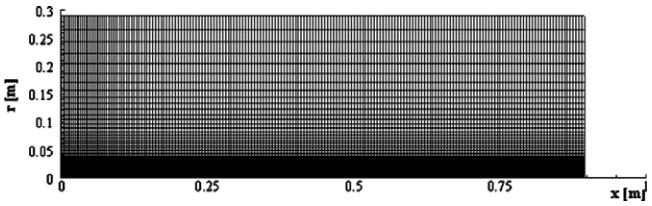

Fig. 3. Computational mesh of the furnace.

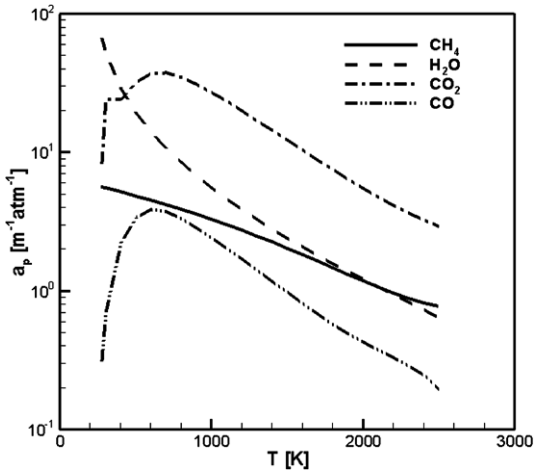

Fig. 4. Planck mean absorption coefficient from RADCAL [33].

radiant intensity emitted by a non-isothermal volume containing non-uniform levels of carbon dioxide, water vapour, methane, carbon monoxide, nitrogen and oxygen. The absorption coefficient of the combined gases is calculated from a narrow-band model and a combination of tabulated spectral properties and theoretical approximations to the vibrational-rotational molecular bands. The CPU time consumed on an Intel Core 2 Duo T7100 1.8 GHz are 56 min for the 6-flux model and 42 min for the P-1 model on the 194 × 86 mesh.

4. Results and discussion

Comparisons between the experimental data reported by Stoomer [21] and the calculated results obtained with and without radiation are shown in Fig. 5 (temperature distribution along the furnace centerline) and Fig. 6 (radial temperature profiles for seven axial locations). No significant differences are observed between the predicted temperatures with and without radiation models near the furnace entrance. This is mainly because the combustion process is at an early stage, maintaining the mean temperature of this zone at low levels. Further downstream, in the main combustion zone ($0.1 < x < 0.4$ m), accounting for radiation effects does not appear to improve agreement with experimental data. Maximum differences in the predicted temperatures on the centerline are of the order of 400 K and can be possibly attributed to the performance of the combustion model.

At the combustor exit (Fig. 5), the maximum predicted centerline temperature is 1440 K without radiation, 1180 K with the 6-flux and 917 K with the P-1 radiation model, corresponding to 18% and 36% decrease respectively. The mean temperature level (Fig. 7) calculated in the high temperature outlet region ($0 \leqslant r \leqslant 0.15$ m, $x = 0.9$ m) is about 671 K without radiation, 611 K with the 6-flux and 556 K with the P-1 radiation model, corresponding to 9% and 17% decrease respectively.

The improvement in agreement with experiments becomes apparent in the high temperature zone ($T >$ 1500 K) extending downstream 400 mm, where the two examined radiation models reduce predicted temperatures by approximately 200 K (6-flux) and 400 K (P-1). Although the overall heat released is the same in all the examined cases, radiative heat transfer is responsible for reducing the size of the high temperature regions of the flame as it is shown by the temperature contours in Fig. 7. A high temperature flame zone is predicted between the injection plane and the main combustion zone in the first half of the furnace length. Temperature levels decrease considerably after this high temperature flame zone until the furnace exit for both radiation models, while high temperatures continue to exist for the no radiation case.

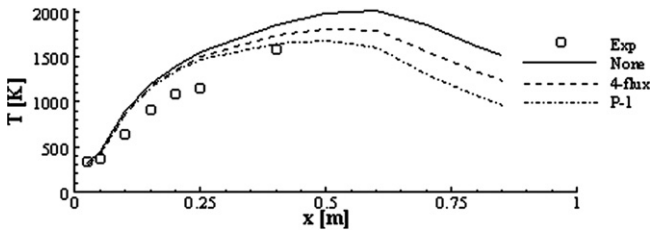

Fig. 5. Temperature distribution along the furnace centerline.

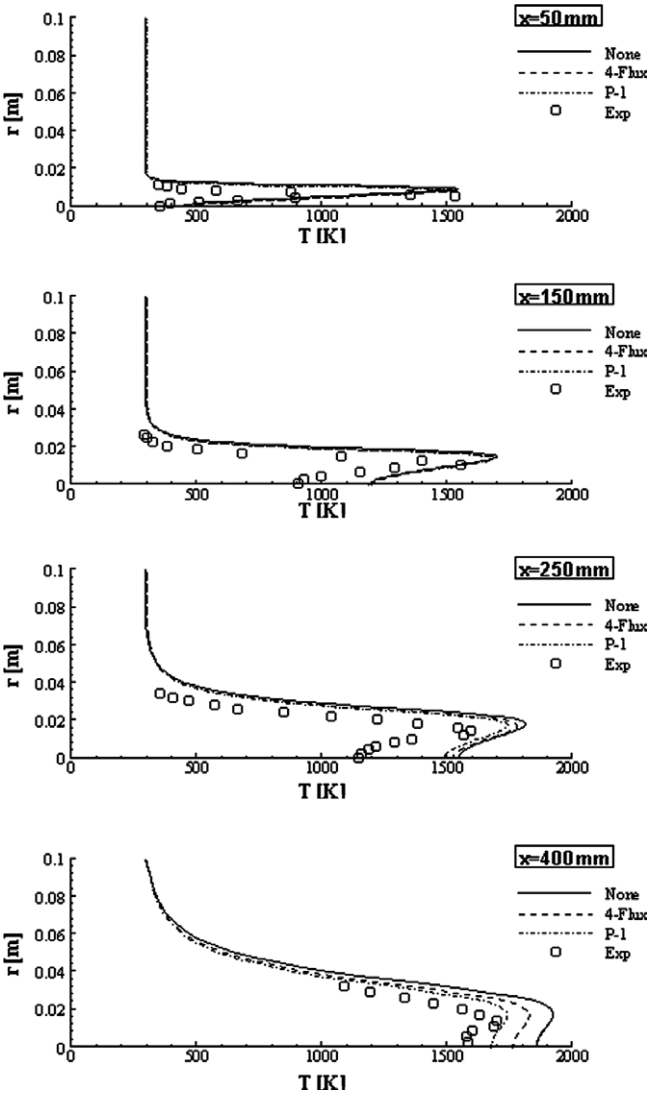

Fig. 6. Radial temperature profiles at distances 50, 150, 250 and 400 mm from entrance.

The predicted radial profiles of the main combustion products (CO_2, H_2O) in the main combustion zone and towards the furnace exit are given in Fig. 8. The predicted profiles show similar trends with the temperature profiles, namely the higher the local temperature the stronger the main products formation. This is due to the fact that towards the furnace outlet the combustion process is kinetically controlled. This implies that in the Arrhenius equation the local temperature directly affects the component rates of production and consumption. At the furnace exit, the predicted maximum CO_2 and H_2O mass fractions are $Y_{CO_2} = 0.093 - Y_{H_2O} = 0.075$ without radiation, $Y_{CO_2} =$

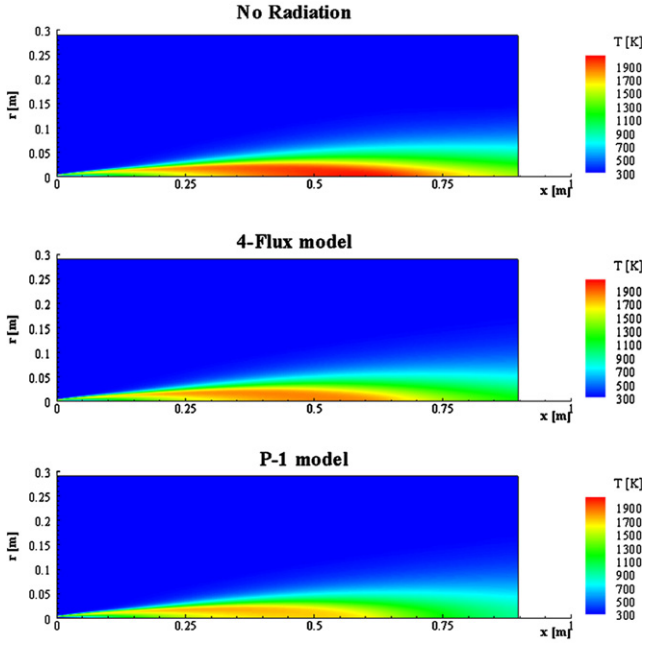

Fig. 7. Contours of temperature.

$0.087 - Y_{H_2O} = 0.071$ with the 6-flux and $Y_{CO_2} = 0.067 - Y_{H_2O} = 0.058$ with the P-1 model. The above highlight the importance of incorporation the appropriate radiation model for the accurate prediction of species concentration.

The contours of the mixture absorption coefficient, as predicted with the 6-flux and the P1 radiation models, respectively, are shown in Fig. 9. Although these two contours are very similar, they are not identical. This is normally expected, as each model predicts a slightly different temperature and composition field inside the furnace. It is noted that the absorption coefficient of the mixture varies from 4.8 to 3.9 m^{-1} (maximum values) just outside the fuel inlet, then it drops to 0.3–1.2 m^{-1} (minimum values) inside the central zone of the combustion process, and just before the combustion gases leave the exit, it rises a little to 1.2–1.5 m^{-1}, following a "3-zone" pattern. The absorption coefficient takes its maximum value, 4.8 m^{-1} just where pure methane is located, at a temperature of 295 K, perfectly agreed to the RADCAL curve, as shown in Fig. 4. As we move inside the main combustion zone, where the main combustion products, CO, CO_2 and H_2O are prevailing and the temperature rises to 1900 K, the absorption coefficient drops rapidly to 0.3 m^{-1}, mainly due to the very high temperature of the combustion products. Finally, as the temperature drops along the exit to 1500 K, the absorption coefficient rises again to 1.2 m^{-1}, making this rise a little more evident with the 6-flux radiation model, which slightly over-predicts local temperatures with respect to the P1 predictions. It is shown that the absorption coefficient of the mixture, as calculated from temperature and composition dependent formulas, varies significantly inside the furnace, a phenomenon which should not be neglected when high-accuracy predictions are sought by the heat transfer engineer.

Overall, in terms of predictive accuracy, P-1 radiation model has performed better than the 6-flux. This can be explained by the fact that the P-1 radiation model takes

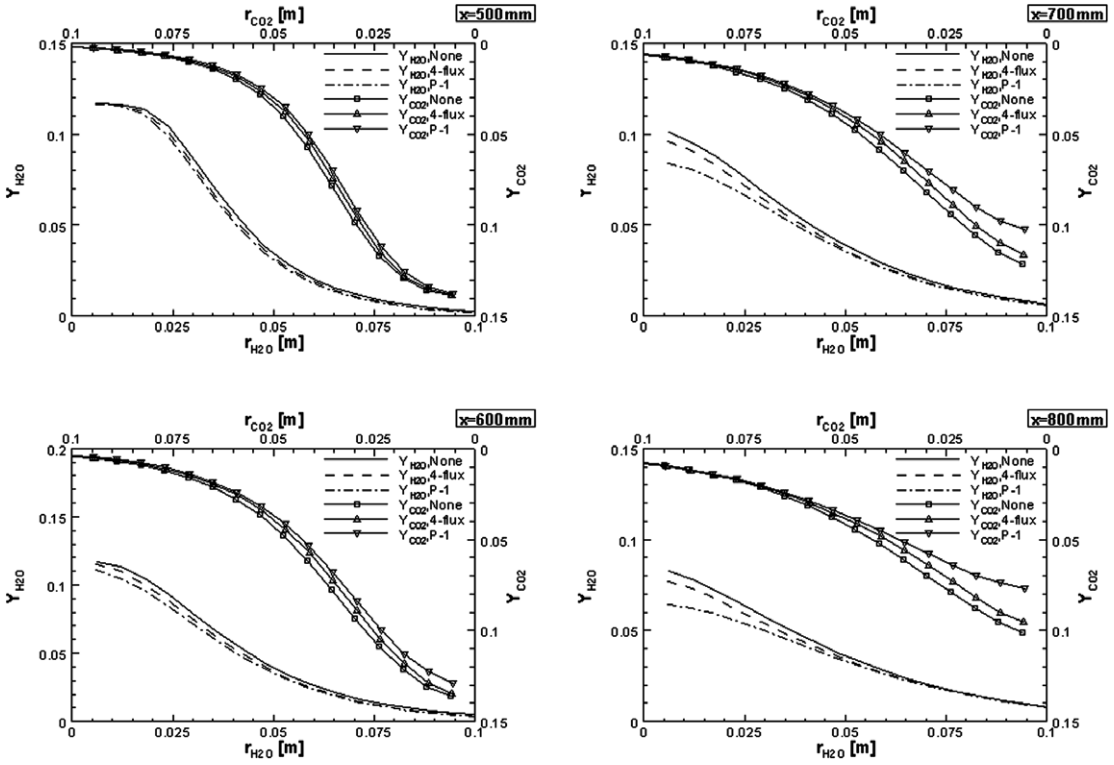

Fig. 8. CO_2 and H_2O radial profiles downstream of furnace.

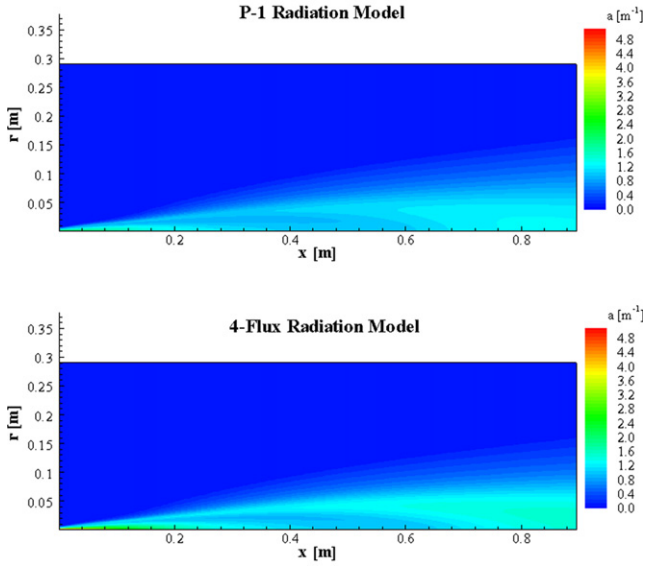

Fig. 9. Contours of absorption coefficient in the combustor.

into account of the integrated radiation intensity in a hemispherical space, expressed through the source term in the P-1 intensity equation (Eq. (13)). On the other hand, the six-flux model is based on a directional selectivity and its accuracy is lower with respect to the P-1 approach when quantities are integrated over the flow geometry. Thus, in the main combustion zone, where high temperature are reached, the six-flux model will 'transmit' radiation to specific directions producing less accurate results. It should also be reminded that the P-1 radiation model offers a significant convenience for engineers, because it can be easily incorporated in any 2-D or 3-D CFD analysis by simply introducing one scalar equation into the calculations (instead of the 6-flux model, where 2 or 3 scalar equations much be introduced) and by setting the appropriate boundary equations.

5. Conclusions

The paper examined numerically a turbulent, non-premixed, natural gas flame with no radiation, with the 6-flux and the P-1 radiation models. As a step forward to current practice hi engineering calculations, the work assessed two computationally low-cost radiation models in a furnace, with steep temperature gradients. Calculation of the absorption coefficients for H_2O, CO_2, CH_4 and CO has been improved by treating them as functions of temperature.

The results confirmed that the effect of radiation is significant on flame temperature and species concentration calculations. As anticipated, the inclusion of thermal radiation in the combustion simulation improved the agreement between predictions and experimental data, with the P-1 model yielding more accurate results, in the case considered. The maximum predicted temperature levels without radiation were higher than those predicted with any of the two radiation models. The inclusion of radiative heat transfer reduced the size of the flame region, where maximum temperatures are located.

Acknowledgements

The project is co-funded by the European Social Fund (75%) and National Resources (25%) – (EPEAEK II) – PYTHAGORAS.

References

[1] H. Guo, Y. Ju, K. Maura, T. Niioka, Radiation extinction limit of counter flow premixed lean methane–air flames, Combust. Flame 109 (1997) 639–646.
[2] A. Abbud-Madrid, D.P. Ronney, Effects of radiative and diffusive transport processes on premixed flames near flammability limits, in: Proceedings of the Twenty-Third International Symposium on Combustion, The Combustion Institute, Pittsburgh, 1990, pp. 423–431.
[3] S.H. Chan, X.C. Pan, M.M.M. Abou-Ellail, Flamelet structure of radiating CH_4-air flames, Combust. Flame 102 (1995) 438–446.
[4] Mustafa Ilbas, The effect of thermal radiation and radiation models on hydrogen–hydrocarbon combustion modelling, Int. J. Hydrogen Energy 30 (10) (2004) 1113–1126.
[5] Mustafa Ilbas, Ilker Yilmaz, Yuksel Kaplam, Investigations of hydrogen and hydrocarbon composite fuel combustion and NO_x emission characteristics in a model combustor, Int. J. Hydrogen Energy 30 (10) (2005) 1139–1147.
[6] A.S. Jamaluddin, P.J. Smith, Predicting radiative transfer in axisymmetric cylindrical enclosures using the discrete ordinates method, Combust. Sci. Technol. 62 (1988) 173–186.
[7] N. Selcuk, Evaluation for radiative transfer in rectangular furnaces, Int. J. Heat Mass Transfer 31 (1988) 1477–1482.
[8] A.C. Ratzell, J.R. Howell, Two-dimensional radiation in absorbing-emitting media using the P–N approximation, ASME J. Heat Transfer 105 (1983) 333–340.
[9] R.G. Siddall, Flux methods for the analysis of radiant heat transfer, J. Inst. Fuel 101 (1974) 101–109.
[10] S.R. Varnas, J.S. Truelove, Simulating radiative transfer in flash smelting furnaces, Appl. Math. Model. 19 (1995) 456–464.
[11] H.C. Hottel, A.F. Sarofim, The effect of gas flow patterns on radiative transfer in cylindrical furnaces, Int. J. Heat Mass Transfer 8 (1965) 1153–1169.
[12] F.R. Steward, P. Cannon, The calculation of radiative heat flux in a cylindrical furnace using the Monte Carlo method, Int. J. Heat Mass Transfer 14 (1971) 245–262.
[13] L.D. Smoot, Pulverized coal diffusion flames: a perspective through modelling, in: Proceedings of the Eighteenth International Symposium on Combustion, The Combustion Institute, Pittsburgh, 1981, pp. 1185–1202.
[14] E.P. Keramida, H.H. Liakos, M.A. Founti, A.G. Boudouvis, N.C. Markatos, Radiative heat transfer in natural gas-fired furnaces, Int. J. Heat Mass Transfer 43 (2000) 1801–1809.
[15] H.H. Liakos, M.A. Founti, N.C. Markatos, Modelling pf stretched natural gas diffusion flames, Appl. Math. Model. 24 (2000) 419–435.
[16] N. Hoffmann, N.C. Markatos, Thermal radiation effects on fires in enclosures, Appl. Math. Model. 12 (1988) 129–140.
[17] S.V. Patankar, D.B. Spalding, in: 14th International Symposium on Combustion, 1981, pp. 1405–1414.
[18] F.C. Lockwood, N.G. Shah, A new radiation solution method for incorporation in general combustion prediction procedures, in: Proceeding of the Eighteenth International Symposium on Combustion, The Combustion Institute, Pittsburgh, 1981, pp. 1405–1416.

[19] P. Cheng, Two-dimensional radiating gas flow by a moment method, AIAA J. 2 (1964) 1662–1664.
[20] R. Siegel, J.R. Howell, Thermal Radiation Heat Transfer, Hemisphere Publishing Corporation, Washington, DC, 1992.
[21] P. Stoomer, Turbulence and OH structure in flames, Ph.D. Thesis, Delft University, Delft, 1995.
[22] A. Klipfel, M.A. Founti, K. Zaehringer, J.P. Martin, J.P. Petit, Numerical simulation and experimental validation of the turbulent combustion and perlite a expansion processes: in an industrial perlite expansion furnace, Flow Turb. Combust. 60 (1998) 283–300.
[23] M.A. Founti, D.I. Kolaitis, Numerical simulation of diesel spray evaporation exploiting the stabilized cool flame phenomenon, Atom. Sprays 15 (2005) 1–18.
[24] D. Kolaitis, M. Founti, Scrutinizing evaporation models for computational modeling of turbulent sprays, in: Proceedings of the Ninth International Conference on Liquid Atomization and Spray Systems (ICLASS 2003), Sorrento, Italy, 2003, pp. 2–18.
[25] S.V. Patankar, Numerical Heat Transfer and Fluid Flow, Hemisphere, New York, 1980.
[26] B.E. Launder, D.B. Spalding, Lectures in Mathematical Models of Turbulence, Academic Press, London, 1972.
[27] B.A. Kader, A.M. Yaglom, Heat and mass transfer laws for fully turbulent wall flows, Int. J. Heat Mass Transfer 15 (1972) 2329–2351.
[28] D.I. Kolaitis, M.A. Founti, A comparative study of numerical models for Eulerian–Lagrangian simulations of turbulent evaporating sprays, Int. J. Heat Mass Transfer 27 (2006) 424–435.
[29] D.I. Kolaitis, M.A. Founti, Modelling of the gas–particle flow in industrial classification chambers for design optimisation, Powder Technol. 125 (2002) 298–305.
[30] B.F. Magnussen, B.H. Hjertager, Proc. Combust. Inst. (1978).
[31] F.L. Dryer, I. Glassman, High temperature oxidation of CO and CH_4, in: 14th International Symposium on Combustion, The Combustion Institute, Pittsburg, 1973.
[32] R.C. Flagan, J.H. Seinfeld, Fundamentals of Air Pollution Engineering, Prentice-Hall, NJ, 1979.
[33] W.L. Grosshandler, RADCAL: A Narrow-Band Model for Radiation Calculations in a Combustion Environment, NIST Technical Note 1402, 1993.